Extended strand characterisation

Xifeng Lu, David M.J. Taylor, Stephen Pragnell
and Damian P. Hampshire

Superconductivity Group, Physics Department,
Durham University, Durham DH1 3LE, UK

Contract. No.: EFDA/05-1296
EFDA Reference TW6-TWSC-STRAIN

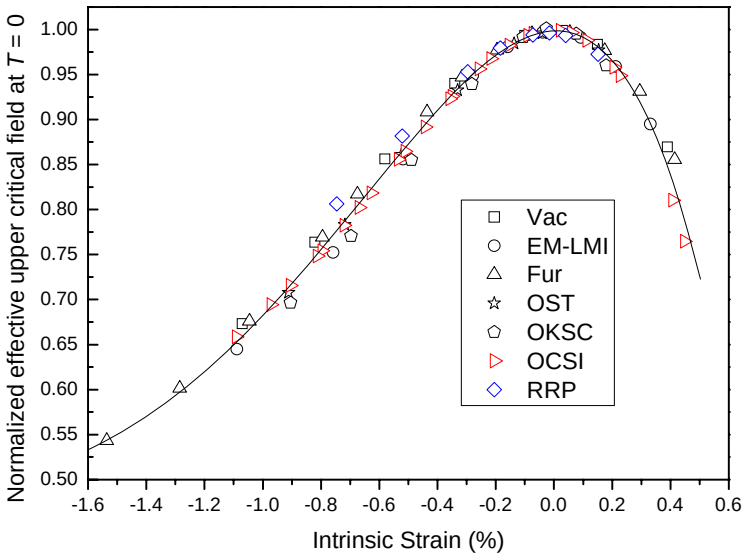

The normalized effective upper critical field at $T = 0$ as a function of intrinsic strain for the OCSI strand and the RRP (Dipole) strand, compared with previous data for five other doped Nb_3Sn strands

Completed June 2007

ACKNOWLEDGEMENTS

The authors acknowledge the help and support of E. Salpietro, A. Vostner, M. Soorie and E. Mossang and the very helpful discussions with R. Zanino.

We also acknowledge the many discussions we have had with those in the community including: D. Bessette, D. Bruzzone, N. Cheggour, J. Duchateau, J. Ekin, W H Fietz, H. Fillunger, B. Karlemo, P. Komarek, R. Maix, N Martovetsky, N. Mitchell, J. Minervini, A. Nyilas, A Nijhuis, A. Portone, K. Osamura, L. Savoldi Richard, J. Schultz and A. Ulbricht.

EXTENDED ABSTRACT

The objective of this task is to provide a comprehensive characterization of an advanced and a high-performance Nb_3Sn strand. The strands measured were the OCSI strand and the RRP Dipole strand also known as the EDIPO strand. Accompanying this report are two spreadsheets that contain tabulations of the J_C and n-value data, as well as the scaling-law parameterisation of $J_C(B,T,\varepsilon)$ and $n(B,T,\varepsilon)$: http://www.dur.ac.uk/superconductivity.durham/publications.html

The extended strand characterizations address and quantify the magnetic field, temperature and strain dependence of the critical current and the n-value. Comprehensive measurements are reported of the engineering critical current density (J_C) at 10 μVm^{-1} as a function of magnetic field, temperature and intrinsic strain. The n-value in the range 10–100 μVm^{-1} was also measured over the same range of parameter space. Consistency tests show that the variable-strain J_C data are homogeneous (±5 %) along the length of the strand, and that there is good agreement between different samples measured in Durham and in other laboratories (at zero applied strain). The OCSI strand has a very similar normalised strain dependence to the OKSC strand. It is found that all the new $J_C(B,T,\varepsilon)$ data are accurately described by the scaling law which was proposed previously and derived using microscopic and phenomenological theoretical analysis. As part of the characterization, strand fitting parameters for J_C have been derived from the evaluation of the experimental data. The relationship between the n-value and critical current (I_C) is also parameterised for both strands using a modified power law of the form $n = 1+rI_C^s$, where r and s are approximately constant.

The OCSI sample is a Nb_3Sn superconducting strand from Luvata Italy, formerly Outokumpu Italy (OCSI). It shows a reversible strain behaviour that is similar to other advanced strand materials (e.g. the OKSC and the OST sample as reported in EFDA03-1126). In contrast although the strain tolerance of J_C for the RRP Dipole strand is somewhat similar to bronze–route and advanced Nb_3Sn strands, the strain range (ε_{rev}) over which J_C is reversible is limited not only up to a maximum tension but also to a maximum compression. Samples were partially damaged when the intrinsic strain (ε_I) was increased beyond ~ -0.77 % in compression and grossly damaged when ε_I was ~ + 0.13 % in tension. This small reversible axial-strain window is an important consideration in the construction and operation of reliable magnets using these very high J_C strands.

Note: RRP Dipole sample S2 was sample Spool 8712-2. Three Dipole RRP samples were measured (at currents up to 600 Amps) that showed the limited reversible elastic window (reported here for the first time).

TABLE OF CONTENTS

1 INTRODUCTION

The J_C versus strain-dependence of Nb_3Sn strands has a significant impact on the final performance of large Cable-in-Conduit Conductors (CICC) like those used in ITER. For any conductor design or performance prediction of CICCs, it is necessary to know the strain dependence of J_C as a function of field and temperature. For several years the Summers Scaling Law was widely accepted and used to describe J_C of Nb_3Sn strands. However, measurements on the Model Coil and recently developed advanced strands have shown significant deviations from the predicted values, especially at high compressive strain. Although the differences between measured and calculated values can be seen as somewhat small they cause very significant uncertainties in the conductor performance extrapolation when it is compared with single strand data. Since the strand layout and composition (binary, ternary or quaternary compounds with Ta and/or Ti) influences the intrinsic strand properties, it is at present not possible to predict accurately the strand performance. As a consequence, it is necessary to measure J_C as a function of field, temperature and strain of each strand type being used in SULTAN samples to have a full set of strand data required for an accurate conductor performance prediction.

One facility capable of measuring the field and strain dependence of the critical strand current at variable temperatures is available here at the University of Durham in Prof. D. P. Hampshire's group. In the framework of the European Fusion Technology programme, the University of Durham has been involved in several strand characterization tasks (e.g. EFDA contracts 02-662 and 03-1126), and thereby has gained a lot of experience in the field of sample preparation, testing and evaluation of the results[1]. The objective of this task is a comprehensive characterization of advanced and high-performance Nb_3Sn strands. The strands measured were the OCSI strand and the RRP strand also known as the Dipole or EDIPO strand.

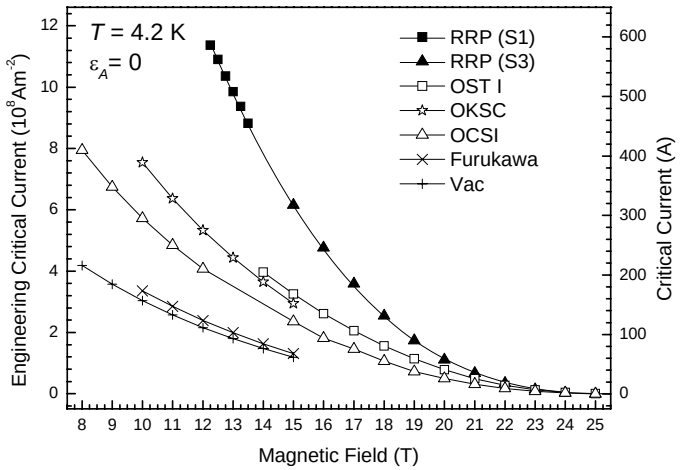

Fig. 1. Engineering critical current density J_C (and critical current I_C) versus magnetic field for Nb_3Sn strands made by different manufactures. The Vac[2] and Furukawa[3] are bronze-route strands. OCSI, OKSC,[4] and OST I[4] are advanced internal-tin strands. The OCSI sample is presented in this report. Samples S1 and S3 are the RRP Dipole strand presented in this report.

There are broadly three different types of Nb_3Sn strand: Bronze-route strands that have low hysteresis losses (< 200 kJm^{-3}) but the engineering J_C (defined as the critical current divided by the total cross-section area of the strand[5]) is also low, typically 250 Amm^{-2} at 4.2 K and 12 T (non-Cu J_C ~ 800 Amm^{-2})[6]; Internal-tin strands of which there are two types - advanced strands with J_C values of ~ 400 Amm^{-2} and losses of ~ 750 kJm^{-3} (acceptable for ITER) and restack-rod-process (RRP) strands for high-energy-physics and NMR, where J_C values of 1200 Amm^{-2} have now been obtained but with very high losses; and powder-in-tube strands which have similar J_C values to those found in RRP strands.[6,7] The bronze-route and two types of internal-tin strand are shown in Fig. 1 – including the OCSI advanced internal-tin Nb_3Sn strand and the RRP internal-tin Nb_3Sn strand that are both the subject of this report.[7]

The remainder of this report is structured as follows: Section 2 outlines the reliability tests and the experimental procedure. Section 3 presents the experimental results, analysis and summary. Sections 3.1 and 3.2 presents the results for the RRP Dipole sample and the OCSI sample respectively; Section 3.3 presents the comparison with other laboratories and samples; Section 3.4 presents the $J_C(B,T,\varepsilon)$ scaling-law parameterization and the parameterisation of the *n*-value data for the two strands. Finally, section 4 presents the summary and conclusions from these data and discusses the physical interpretation of the results.

2 EXPERIMENTAL PROCEDURE

2.1 Samples and heat-treatments in the furnace

Measurements were performed on two types of chrome-plated Nb_3Sn strands: a Dipole RRP strand and a Luvata (OCSI) strand. Three Dipole RRP 0.81 mm diameter Nb_3Sn strands with 91 subelements were measured. Samples S1 and S3 were reacted together and separately from sample S2. Samples S1 and S2 were measured using the superconducting magnet (B < 15 T) in Durham. Sample S3 was measured in Grenoble in magnetic fields up to 28 T. Two ITER-candidate OCSI samples of diameter 0.81 mm were also measured. They were both reacted at the same time – one sample was measured at 4.2 K, the other at temperatures above 4.2 K.

All strands were heat-treated in an argon atmosphere on oxidised stainless-steel mandrels in a three-zone furnace, with an additional thermocouple positioned next to the sample in order to monitor the temperature using the heat-treatment schedules shown in Table I. The wires were then etched in hydrochloric acid to remove the chrome and transferred to nickel-plated Ti–6Al–4V helical springs, to which they were attached by copper plating and soldering. The helical springs used for both strands have the same optimised four-turn tee-shaped cross-section[8,9].

Dipole RRP strand	OCSI strand
Ramp at 10°C h^{-1} to 210°C and hold for 48 h	Ramp at 10° C h^{-1} to 185°C and hold for 24 h
Ramp at 10° C h^{-1} to 400°C and hold for 48 h	Ramp at 50° C h^{-1} to 460°C and hold for 48 h
Ramp at 10° C h^{-1} to 640°C and hold for 60 h	Ramp at 50° C h^{-1} to 575°C and hold for 100 h
Ramp at 10° C h^{-1} to room temperature	Ramp at 50° C h^{-1} to 650°C and hold for 175 h
	Ramp at 25° C h^{-1} to room temperature

Table I Heat-treatment schedules for the RRP Dipole and OCSI strands.

2.2 Using the Durham $J_C(B,T,\varepsilon)$ probe

The Durham strain probe[8,10] was used to carry out voltage–current (V–I) measurements on the strands as a function of magnetic field (B), temperature (T) and applied axial strain (ε_A). The measurements involved monitoring the voltage across sections of the sample as a function of the current through it. J_C (or I_C) was measured (is defined) at an electric field criterion of 10 μVm^{-1}.

The spring is twisted to apply the strain to the wire via concentric shafts: the inner shaft connects a worm-wheel system at the top of the probe to the top of the spring, and the outer shaft is connected to the bottom of the spring via an outer can. For measurements at 4.2 K, the outer can contains a number of holes to admit liquid helium from the surrounding bath, whereas for measurements above 4.2 K, the outer can forms a vacuum space around the sample with a copper gasket and knife edge seal between the can and the outer shaft. In this case, the temperature is controlled via three independent Cernox thermometers and constantan wire heaters[11]. Temperatures below 4.2 K were obtained by pumping on the liquid helium and controlling the pressure and monitoring the temperature using the 3 Cernox thermometers. Using this method we obtained measurements at 2.35 K on the OCSI sample. The detailed description of the experimental apparatus and techniques can be found elsewhere [5,8,10,12].

The measurement were made in fields up to 15 Tesla in Durham and in magnetic fields up to 28 T using the resistive magnets at the European LCMI-CNRS High-field Laboratory in Grenoble, France.

2.3 Reliability of the $J_C(B,T,\varepsilon)$ data

Broadly we use 4 tests to assess whether the strand has been damaged and hence whether the J_C data are reliable. Initially we measure I_C at 4.2 K and a few magnetic fields to confirm the specifications of the manufacturer. For the RRP strand, I_C was 586 A ± 3 % at 4.2 K, and 12.25 T (cf Fig. 1) which is within 1 % of the manufacturer's nominal value. Throughout the experiment we check: the homogeneity of the strand - typically five different sections of the strand are measured, each approximately 20 mm long; the flat (zero-resistance) baseline of the V-I data, to ensure it is within the noise of our measurement (typically a few nanovolts); and the reversibility of the sample, by

measuring whether or not $J_C(B,T,\varepsilon)$ at zero applied strain is reversible to better than 3-4 %. We have made comprehensive measurements on ITER bronze-route and other advanced internal-tin strands (eg OST) in the applied strain range -1.5 % $\leq \varepsilon_A \leq$ +0.5 %, including strain cycling, without producing any damage.[1]

3 RESULTS AND ANALYSIS

This report presents critical current (I_C) and engineering critical current density (J_C) data defined at an electric-field criterion of 10 μVm^{-1}, where the latter is calculated by dividing the critical current by the total cross-sectional area of the wire (5.153×10^{-7} m^2).

3.1 Dipole sample raw data (3 samples)

3.1.1 $J_C(B,T,\varepsilon)$ data

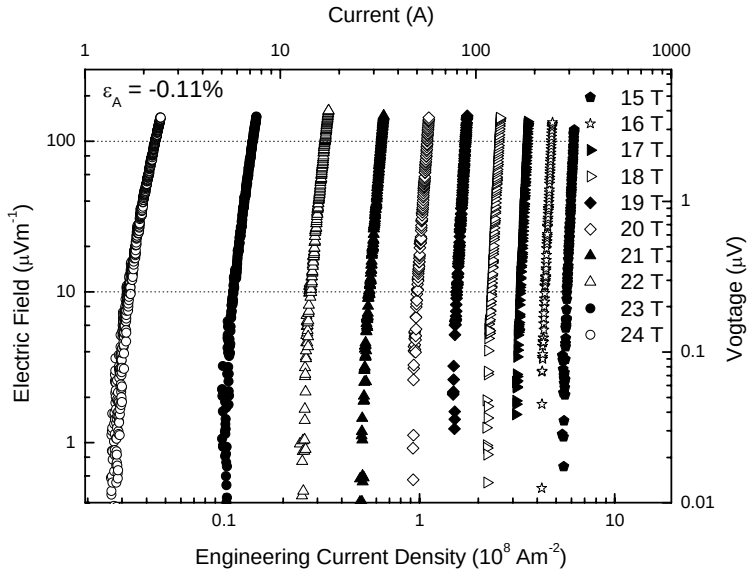

Fig. 2. Log-log plot of electric field versus engineering current density (and voltage versus current) for the RRP Dipole strand at 4.2 K, with ε_A = -0.11 % and integer magnetic fields between 15 and 24 T.

Figure 2 shows typical electric field–current density (*E-J*) (and voltage–current: *V-I*) characteristics measured at 4.2 K and ε_A = -0.11 %. The noise in these measurements is a few nanovolts – primarily the Johnson noise from the voltage taps. It is clear that these characteristics are not straight lines. Nevertheless for magnet engineering purposes, it is

helpful to find *n*-values which are calculated using the power law expression $E = \alpha J^n$ with E between 10 and 100 μVm^{-1}.

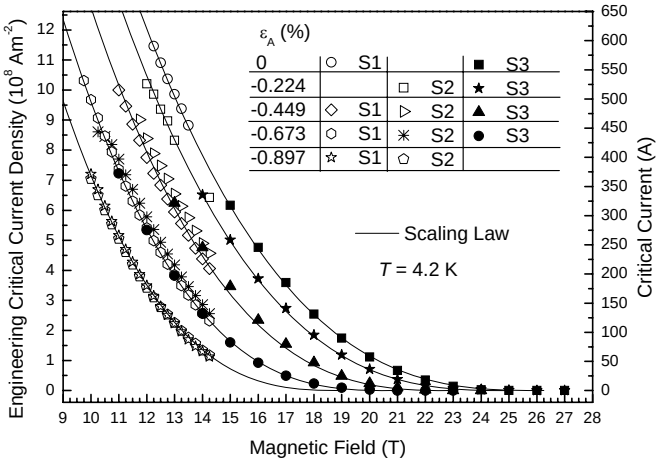

Fig. 3. Engineering critical current density (and critical current) as a function of magnetic field at 4.2 K for the RRP Dipole samples S1, S2 and S3. The lines are provided by the scaling law.[1]

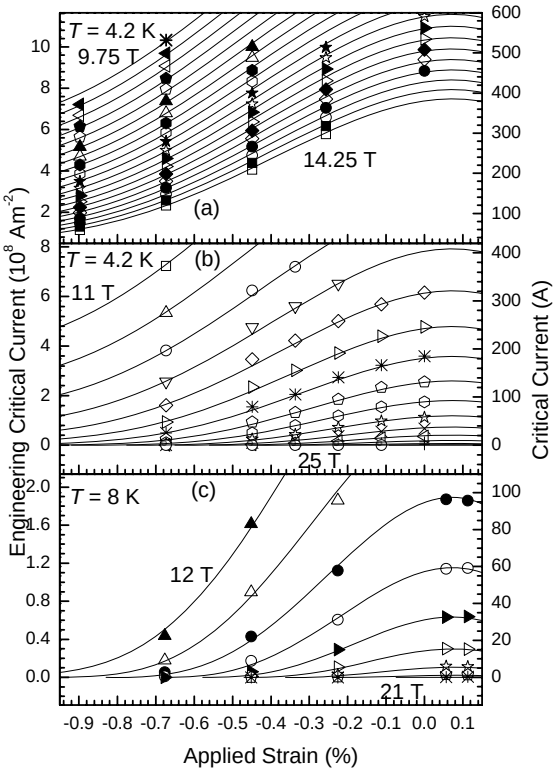

Fig. 4. Engineering critical current density (and critical current) as a function of applied strain at 4.2 K and 8 K for the Dipole RRP strand. (a) Sample S1 in magnetic fields from 14.25 to 9.75 T in increments (ΔB) of 0.25 T at 4.2 K. (b) and (c) Sample S3 at 4.2 K and 8 K (ΔB = 1 T) respectively. The lines are provided by the scaling law.[1]

Fig. 3 shows engineering critical current density (and critical current) as a function of magnetic field at 4.2 K for the three RRP Dipole samples S1, S2 and S3. Good agreement between the J_C (and I_C) values and the mechanical properties is found for all three RRP samples studied. For samples S1 and S2, once the applied compressive strain was increased beyond ~ -0.7 %, the J_C of the strands were not homogeneous, consistent with partial damage. Homogeneity tests on different sections showed that increased compressive strain down to $\varepsilon_A \sim$ -0.9 %, caused progressively more damage. As the damage increased we found that some sections began to quench over some limited field ranges so that I_C could not be measured. Figure 4(a) is a plot of J_C (and I_C) as a function of applied strain at 4.2 K for S1 for magnetic fields at and below 14.25 T with field increments of 0.25 T. At $\varepsilon_A \sim$ -1.1 %, a shaft in the probe failed which prevented further measurements on S1. For sample S2, after the compressive measurements at 4.2 K, measurements were made at 8 K and 12 K. Further compressive measurements (at these higher temperatures) caused further damage and a reduction in I_C of about 15 % from the original values. Then tensile strain was applied. At ε_A ~ +0.2 % gross damage occurred - one section was completely resistive, others had very low J_C values and some were not measurable (i.e. quenched). Given S1 and S2 were both damaged at ~ -0.7 % we restricted measurements on S3 at 4.2 K to ~ -0.7 % < $\varepsilon_A \leq$ 0 %. Good homogeneity and flat baselines for the *V-I* data were found. Then variable temperature measurements were made at 8, 10, and 14 K over the same compressive range. At $\varepsilon_A \sim$ -0.7 %, one of the five sections for S3 was damaged although the others remained reversible. Figs. 4(b) and 4(c) show J_C values for S3 at 4.2 K and 8 K. As with S2, once ε_A was increased (in tension) to ~ +0.2 %, S3 was seriously damaged. Hence we conclude that all 3 samples showed evidence for partial damage when the applied compression was increased beyond ~ - 0.7 % and the two samples measured in tension showed gross damage at ~ +0.2 %. To our knowledge, this is the first report of a reversible limit in an axial compression measurement of J_C. Gross damage on applying a small tension to these strands has been observed independently by two other groups.[13]

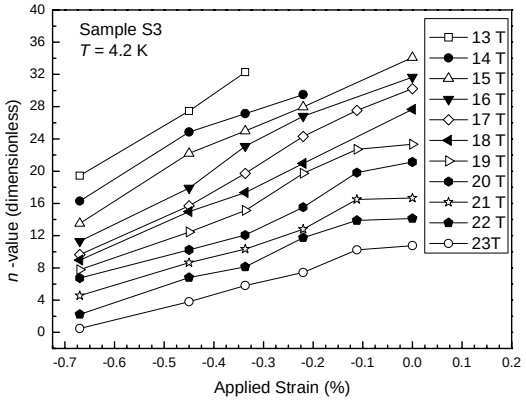

Fig. 5: The *n*-value obtained from fitting the experimental data to the equation $E = \alpha J^n$ over the range from 10 to 100 μVm^{-1}. Data are shown for the RRP Dipole strand at 4.2 K as a function of strain and magnetic field.

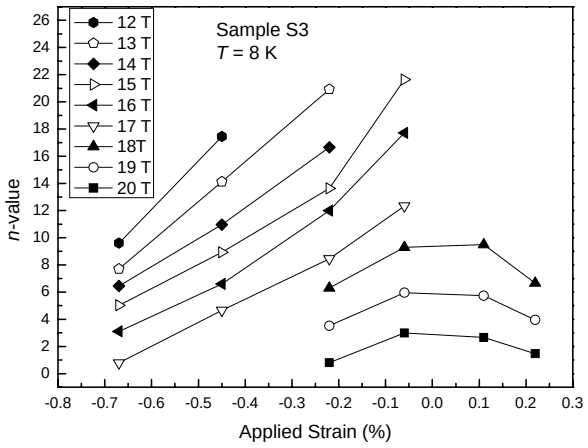

Fig. 6: The *n*-value obtained from fitting the experimental data to the equation $E = \alpha J^n$ over the range from 10 to 100 μVm^{-1}. Data are shown for the RRP Dipole strand at 8 K as a function of strain and magnetic field.

3.1.2 $n(B,T,\varepsilon)$ data

Using the power-law expression $E = \alpha J^n$ and fitting the *E*-*J* data over the range from 10 to 100 μVm^{-1}, values of *n* were obtained. It can be seen in Figs. 5 and 6 that the strain–dependence of the *n*-value has a similar inverted parabolic behaviour to critical current density as has been observed before. In section 3.4, we parameterise the *n*-values in terms of the critical current.

3.2 OCSI sample raw data

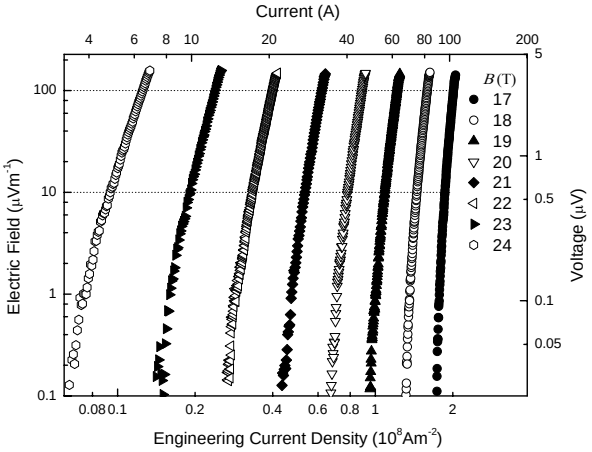

Figure 7. Log-log plot of electric field versus engineering current density (and voltage versus current) for the OCSI strand at temperature of 2.35 K, with ε_A = -0.14 % and integer magnetic fields between 17 and 24 T.

3.2.1 $J_C(B,T,\varepsilon)$ data

Figure 7 shows electric field–current density (*E*-*J*) (and voltage–current: *V*-*I*) characteristics measured at 4.2 K and ε_A = -0.14 % on log-log plots. As with the RRP Dipole data the noise is a few nanovolts. The *n*-values were calculated and are presented below in section 3.2.2.

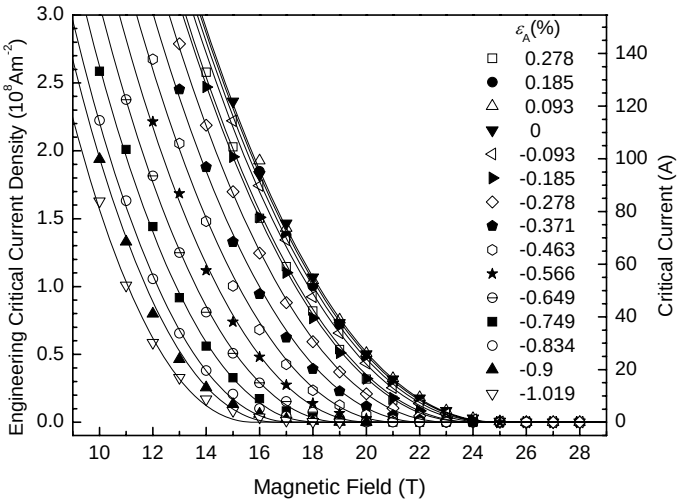

Figure 8. Engineering critical current density (and critical current) as a function of magnetic field at 4.2 K with ε_A from -1.019 % to +0.278 %. for the OCSI strand. The lines are provided by the scaling law.

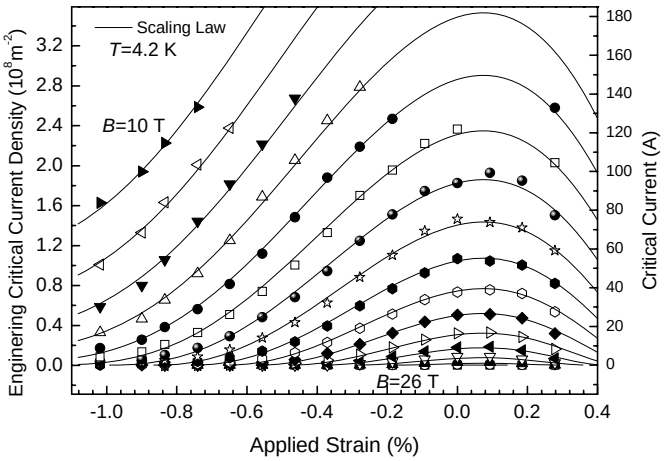

Figure 9. Engineering critical current density (and critical current) as a function of applied strain at 4.2 K and integer magnetic fields between 10 and 26 T for the OCSI strand. The lines are provided by the scaling law.

Figure 8 shows J_C (and I_C) as a function of magnetic field at 4.2 K with variable applied strain ($-1.1\ \% \le \varepsilon_A \le +0.28\ \%$). Figure 9 shows J_C (and I_C) as a function of applied strain at 4.2 K in fields up to 26 Tesla ($10\ \text{T} \le B \le 26\ \text{T}$). Figure 9 shows how sensitive J_C is to strain and the well-known asymmetry in which J_C is more sensitive to the tensile strain than to the compressive strain.

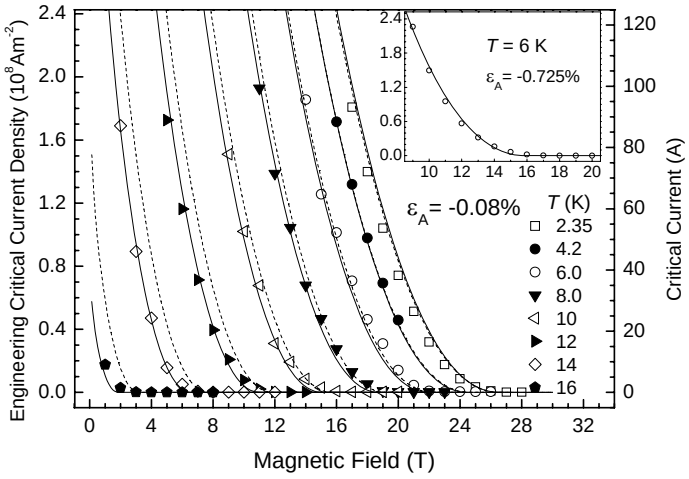

Figure 10. Engineering critical current density (and critical current) as a function of magnetic field with temperature from 2.35 K to 16 K for the OCSI strand. The solid lines are provided by the scaling law using parameters listed in table III. The dotted lines are the scaling law that is found if data at 4.2. K alone and a T_C of 17.5 K is used. The inset is the measured J_C versus magnetic field at 6 K with ε_A = -0.725 %.

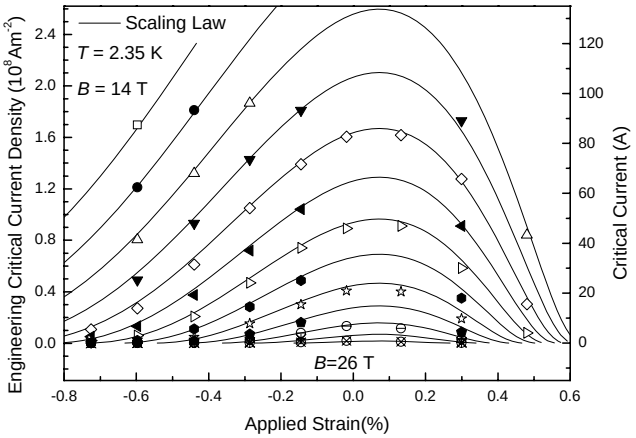

Figure 11. Engineering critical current density (and critical current) as a function of applied strain at $T = 2.35$ K for the OCSI strand. The lines are provided by the scaling law.

Figure 10 shows J_C (and I_C) as a function of magnetic field from temperature 2.35 K to 16 K. The effect of temperature on J_C is illustrated clearly. The inset of Fig. 10 shows J_C as a function of magnetic field at 6 K with ε_A = -0.725 %. Fig. 11 shows that the scaling law fits the data well at 2.35 K. To our knowledge, this is the first time variable-strain J_C measurements have been made below 4.2 K on Nb_3Sn superconducting strands.

3.2.2 $n(B,T,\varepsilon)$ data

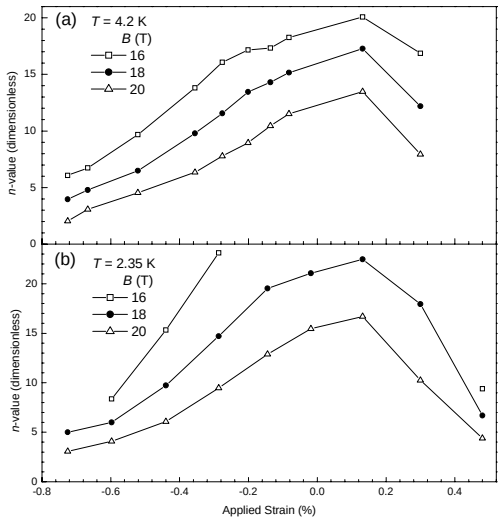

Fig. 12: The n-value obtained from fitting the experimental data to the equation $E = \alpha J^n$ over the range from 10 to 100 μVm^{-1}. Data are shown for the OCSI strand at 4.2 K and 2.35 K as a function of strain and magnetic field.

As with the RRP Dipole sample, we have used the *E-J* data (for example shown in Fig. 7) to fit the power-law expression $E = \alpha J^n$ over the range from 10 to 100 μVm^{-1}, to obtain values of *n*. Typical values of *n* are shown in Fig. 12 and parameterised in terms of critical current in section 3.4.

3.3 Comparisons with other laboratories and other samples

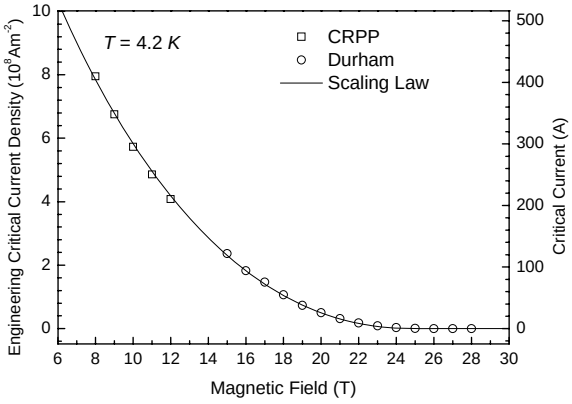

Fig. 13. Interlaboratory comparisons of the critical current of the OCSI strand at zero strain and 4.2 K as a function of magnetic field compared with the data from CRPP. The line is provided by the scaling-law.

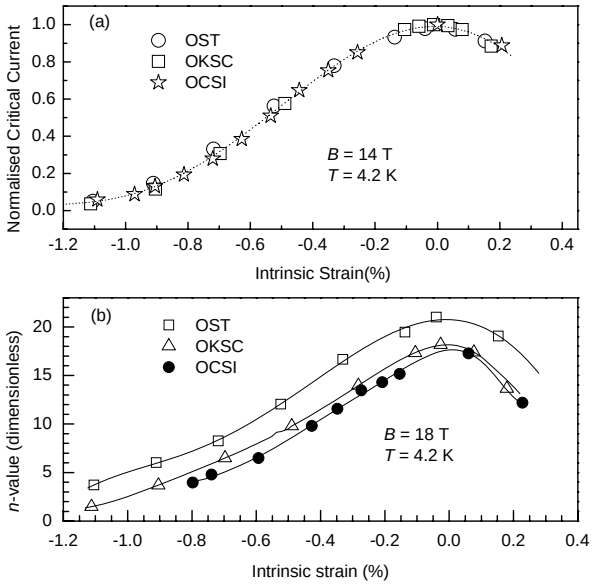

Fig. 14. Comparisons of the critical current of the OST[2], OKSC [4] and OCSI strand at 4.2 K. (a) Normalised critical current as a function of strain at 14 T. (b) *n*-value as a function of strain at 18 T. The lines are a guide to the eye.

An inter-laboratory comparison of J_C data obtained in Durham with that measured by CRPP (Center for Research in Plasma Physics of Switzerland) is shown in Fig. 13. All data are in broad agreement with the scaling law. Figure 14 shows the normalized critical current as a function of intrinsic strain at B = 14 T and the n-value at 18 T and 4.2 K, where intrinsic strain $\varepsilon_I = \varepsilon_A - \varepsilon_M$ and ε_I is by definition zero when J_C is a maximum. Excellent agreement is found between the OKSC and the OCSI samples which were made with similar manufacturing techniques. These two strands also have a similar strain dependence to the OST and RRP Dipole strand.

3.4 Critical current density data and *n*-value parameterisation

The $J_C(B,T,\varepsilon)$ data at 10μVm^{-1} are parameterised using the scaling law described previously[1], which involves the following relations:

$$J_C(B,T,\varepsilon_I) = A(\varepsilon_I)\left[T_C^*(\varepsilon_I)\left(1-t^2\right)\right]^2\left[B_{C2}^*(T,\varepsilon_I)\right]^{n-3} b^{p-1}(1-b)^q \quad (1)$$

$$B_{C2}^*(T,\varepsilon_I) = B_{C2}^*(0,\varepsilon_I)\left(1-t^\nu\right) \quad (2)$$

$$\left(\frac{A(\varepsilon_I)}{A(0)}\right)^{1/u} = \left(\frac{B_{C2}^*(0,\varepsilon_I)}{B_{C2}^*(0,0)}\right)^{1/w} = \frac{T_C^*(\varepsilon_I)}{T_C^*(0)} \quad (3)$$

$$\frac{B_{C2}^*(0,\varepsilon_I)}{B_{C2}^*(0,0)} = 1 + c_2\varepsilon_I^2 + c_3\varepsilon_I^3 + c_4\varepsilon_I^4, \quad (4)$$

$$\varepsilon_I = \varepsilon_A - \varepsilon_M, \quad (5)$$

where J_C is the engineering critical current density (the critical current divided by the total cross-sectional-area of the wire), ε_A is the applied strain, ε_I is the intrinsic strain, ε_M is the applied strain at the peak, T_C^* is the effective critical temperature, $t = T/T_C^*$ is the reduced temperature, B_{C2}^* is the effective upper critical field and $b = B/B_{C2}^*$ is the reduced field.

The n-value is defined via the following relation:

$$E = \alpha J^n, \quad (6)$$

where E is the electric field and J is the (engineering) current density. A tabulation of the $J_C(B,T,\varepsilon)$ and $n(B,T,\varepsilon)$ data can be found in the spreadsheet that accompanies this report[14].

The n-value is used to characterize the sharpness of the E-J transition in technological superconductors [15]. It is commonly used as a 'quality index' for the superconducting materials [16]. The functional form of the n-value is particularly similar to the OKSC sample and broadly similar to the OST and RRP Dipole strands. It is known that some extrinsic factors, for example, the cylindrical uniformity of the filaments can effect the n-value. Equally intrinsic factors are also known to play a role. Given the similar inverted parabolic behaviour found for both n and the critical current as well as the experimental result that n approaches to 1 as I_C to zero, the relationship between n-value and the critical current is parameterised using the following modified power law [2],

$$n(B,T,\varepsilon_1) = 1 + r(T,\varepsilon_1)\left[I_C(B,T,\varepsilon_1)\right]^{s(T,\varepsilon_1)} \quad (7)$$

3.1.1 Parameterisation of the RRP Dipole strand

p	q	***n***	***v***	***w***	***u***	ε_M (%)
1.0404	2.913	***2.500***	***1.500***	***2.200***	***0***	0.0722
$A(0)$ ($Am^{-2}T^{3-n}K^{-2}$)		$T_C^*(0)$ (K)	$B_{C2}^*(0,0)$ (T)	c_2	c_3	c_4
1.493×10^8		16.90	30.20	−0.6362	−0.4346	−0.0578

Table II. Scaling law[1] parameters for the RRP strand derived from variable strain, field and temperature data. The four parameters in bold were not varied in the fitting procedure.[1]

Using the reversible data obtained on samples S1 and S3, we have parameterised $J_C(B,T,\varepsilon)$ using the scaling law cited above[1]. All parameters and constants obtained from fitting all the data to the scaling law are given in the table II (parameters in bold are not varied in the fitting procedure).[1] First the variable temperature data above 4.2 K, which includes data at strains above and below the peak in J_C were used to obtain an accurate value of ε_M. Then a global fit to all the data, provided the best-fit values for the other free-parameters. The lines in all figures showing J_C data were generated using the scaling-law and demonstrate it fits the data well. Since J_C peaks when $\varepsilon_A = \sim 0.07$ %, the

small reversible strain window can be expressed in terms of an intrinsic (rather than applied) strain window of -0.77 % to +0.13 % where the intrinsic strain is defined to be zero when J_C reaches it peak value.

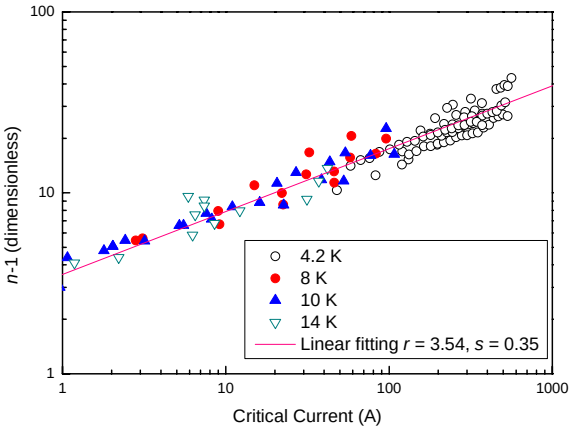

Fig. 15: The *n*-value obtained from fitting the experimental data to the equation $E = \alpha J^n$ over the range from 10 to 100 μVm^{-1}. Data are shown for the RRP Dipole strand at 4.2 K, 8 K, 10 K and 14 K as a function of strain and magnetic field.

The *n*-value data have been replotted in Fig. 15 on a *n*-1 as a function of I_C plot. As with other Nb_3Sn strands it is found $r(T,\varepsilon)$ and $s(T,\varepsilon)$ are approximately constant (3.54 and 0.35 respectively).

3.1.1 Parameterisation of the OCSI strand

p	q	$\boldsymbol{n}$	$\boldsymbol{\nu}$	$\boldsymbol{w}$	$\boldsymbol{u}$	ε_M (%)
0.9012	2.162	***2.500***	***1.500***	***2.200***	***0***	0.0718
$A(0)$ (Am^{-2}T^{3-n}K^{-2})		$T_C^*(0)$ (K)	$B_{C2}^*(0,0)$ (T)	c_2	c_3	c_4
3.231×10^7		16.88	28.56	−0.8216	−0.6941	−0.1867

Table III. Scaling law parameters for the OCSI strand derived from variable strain, variable field and variable temperature data. The RMS difference between the measured and parameterized values is 1.91 A. Four of the parameters whose values are given in bold were not varied in the fitting procedure.

The $J_C(B,T,\varepsilon)$ data were parameterized by the above scaling law. The parameters in table III describe accurately all the data from 2.35 K to 16 K (see solid lines in all figures that present $J_C(B,T,\varepsilon)$ data). The RMS difference between the measured and parameterized values for all of the available data is 1.91 A.

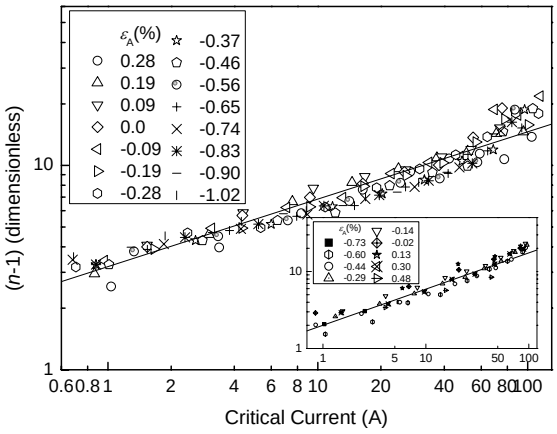

Fig. 16. n-1 as a function of critical current at T = 4.2 K and T = 2.35 K (the inset). The lines show a universal fit made using equation (7).

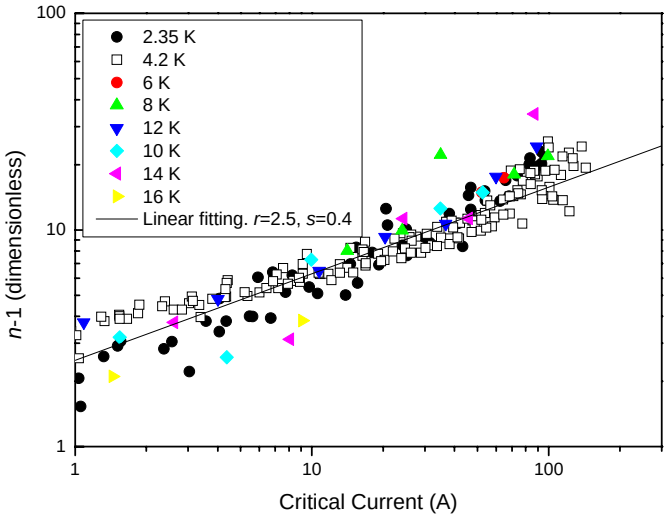

Fig. 17: The n-value obtained from fitting the experimental data to the equation $E = \alpha J^n$ over the range from 10 to 100 μVm^{-1}. Data are shown for the OCSI strand at 2.35, 4.2, 6, 8, 10, 12, 14 and 16 K as a function of strain and magnetic field.

The *n*-value data for the OCSI strand have been plotted in Figs. 16 and 17 as *n*-1 as a function of I_C. The best fit for the parameters *r* and s have been calculated and are presented in table IV.

	Dipole RRP strand	OCSI strand
$r(T,\varepsilon)$	3.54	2.5
$s(T,\varepsilon)$	0.35	0.4

Table IV The parameters *r* and *s* (derived from the *n*-value data in Figs. 14 and 16) for the RRP Dipole and OCSI strands.

4 SUMMARY AND CONCLUSIONS

In the reversible range, both the RRP Dipole sample and the OCSI sample can be characterised by the scaling law for J_C and the power law for the index *n*. The parameters which are derived from these fits are provided in tables II, III and IV above.

Bronze-route strands and the advanced OCSI strands are characterised by well-defined filaments and low losses. Although when reacted at ambient pressure, bronze-route strands show Kirkendale voids, these voids are completely eliminated in reactions at 1300 bar using Hot-isostatic-pressing (HIP) and a significant increase occurs in the tensile strain at which damage first appears.[17] In the RRP strands, the sub-elements have a very different structure to both bronze-route and advanced OCSI internal-tin strands because the individual filaments coalesce[7] (so the losses are high) to form a thick superconducting layer. The RRP strands also have significant porosity both within the Nb_3Sn layer and the Sn reservoir.[18] We suggest that crack propagation starts at lower tensile and compressive strains because of the porosity and voids present in or near the thick superconducting layers in the RRP strands. Cracks tend to propagate across the superconducting current path in tension whereas in compression they propagate along the current path. Hence, consistent with the experimental data, there are gross changes in J_C

(and gross damage) when cracks first propagate in tension compared to limited damage in compression.

To a first approximation, the normalised strain tolerance of J_C in RRP strands is somewhat similar to the OCSI Nb_3Sn strands as well as those made by other fabrication routes, indicated by the good fits obtained using the scaling law. This is consistent with attributing the strain tolerance of J_C primarily to the strain tolerance of the fundamental critical superconducting parameters - hence the porosity and voids present in RRP strands have little effect.

This is the first report of the detailed scaling law data in the reversible range for a RRP strand and an OCSI strand. $J_C(B,T,\varepsilon)$ data fit the standard scaling law and have a similar field, axial strain and temperature tolerance to other ITER candidate strands.[1] The n-values can also be parameterised using a standard power law. To our knowledge, this is the first observation of a reversible strain window - the strand can be damaged not only in tension but also in compression. Further studies are needed to confirm the range of the strain window we have seen in three samples and also to identify where the crack initiation sites are located, what the reversible strain window for these RRP Dipole strands is in response to bending strains and whether the strands can be improved for example by HIP'ing.[17,19]

5 REFERENCES

1 D M J Taylor and D P Hampshire, "The scaling law for the strain dependence of the critical current density in Nb_3Sn superconducting wires," Supercond. Sci. Tech. 18, S241-S252 (2005).

2 D M J Taylor and D P Hampshire, "Relationship between the *n*-value and critical current in Nb_3Sn superconducting wires exhibiting intrinsic and extrinsic behaviour," Supercond. Sci. Tech. 18, 297-302 (2005).

3 D P Hampshire, D M J Taylor, P Foley et al., Report No. DurSC0601, 2001.

4 D M J Taylor and D P Hampshire, Report No. EFDA-03-1126, 2005.

5 S A Keys and D P Hampshire, in *Handbook of Superconducting Materials*, edited by D Cardwell and D Ginley (IOP Publishing, Bristol, 2003), Vol. 2, pp. 1297-1322.

6 A. Vostner and E. Salpietro, "Enhanced critical current densities in Nb_3Sn superconductors for large magnets," Superconductor Science & Technology 19, S90-S95 (2006).

7 S Hong, M B Field, J A Parrell et al., "Latest improvement of Current Carrying Capability of Niobium Tin and Its Magnet Applications," IEEE Trans. Appl. Supercond. 16 (2), 1146-1151 (2006).

8 D M J Taylor and D P Hampshire, "Properties of helical springs used to measure the axial strain dependence of the critical current density in superconducting wires," Supercond. Sci. Tech. 18, 356-368 (2005).

9 C R Walters, I M Davidson, and G E Tuck, "Long sample high sensitivity critical current measurements under strain," Cryogenics 26, 406-412 (1986).

10 N Cheggour and D P Hampshire, "A probe for investigating the effects of temperature, strain, and magnetic field on transport critical currents in superconducting wires and tapes," Rev. Sci. Instrum. 71 (12), 4521-4530 (2000).

11 B L Brandt, D W Liu, and L G Rubin, "Low temperature thermometry in high magnetic fields. VII Cernox^{TM} sensors to 32 T," Rev. Sci. Instrum. 70, 104-110 (1999).

12 S A Keys, N Koizumi, and D P Hampshire, "The strain and temperature scaling law for the critical current density of a jelly-roll Nb_3Al strand in high magnetic fields," Supercond. Sci. Tech. 15, 991-1010 (2002).

13 A Vostner, Private communication. EFDA magnet experts workshop Barcelona (2007).

14 http://www.dur.ac.uk/superconductivity.durham/.

15 P Bruzzone, "The index n of the voltage–current curve, in the characterization and specification of technical superconductors," Physica C 401 (1-4), 7-14 (2004); D P Hampshire and H Jones, "Critical current of a NbTi reference material as a function of field and temperature," Magnet Technology 9, 531-535 (1985).

16 A K Ghosh, "*V-I* transition and *n*-value of multifilamentary LTS and HTS wires and cables," Physica C 401 (1-4), 15-21 (2004).

17 T Fukutsuka, T Horiuchi, Y Monju et al., "Effects of hot isostatic pressing on the superconducting properties of Nb_3Sn multifilamentary wires," Adv. Cryo. Eng. 30, 891- 898 (1984).

18 P J Lee and D C Larbalestier, "Microstructure, Microchemistry and the Development of Very High Nb_3Sn Layer Critical Current Density," IEEE Trans. Appl. Supercond. 15 (2), 3474 - 3477 (2005).

19 S A Keys, N Cheggour, and D P Hampshire, "The effect of hot isostatic pressing on the strain tolerance of the critical current density found in modified jelly roll Nb_3Sn wires," IEEE Trans. Appl. Supercond. 9 (2), 1447-1450 (1999).